Relativistic Dynamics

Eric R. Chen*
MIT Department of Physics
(Dated: June 20, 2020)

In the early 1900's, one of the biggest challenges in physics was bridging the contradictions between Newtonian Mechanics and the Maxwell theory of the electromagnetic field when applied to a charged particle moving at high speed. When Einstein published his seminal paper *On the Electrodynamics of Moving Bodies*[1], the resulting model of relativistic dynamics provided an alternative to classical mechanics in predicting the relationship between the motion and properties of a high velocity particle. In this experiment, we measure and relate the energy K, momentum $\vec{p}$ and velocity $\vec{v}$ of an electron moving at 60% to 80% the speed of light c in order to demonstrate that these relationships for such an object are predicted by the relativistic model as opposed to the classical model. From our measurements, we extract the electron charge to mass ratio to be $\frac{e}{m_e} = (4.69 \pm 0.043)e^{17}$ $(\frac{esu}{g})$.

I. THEORY OF NEWTONIAN AND RELATIVISTIC DYNAMICS

The Theory of Special Relativity introduced by Einstein [1] allows us to derive relationships between the momentum, velocity and energy of a particle moving at high speed which differ from the classical model. In order to determine which model best predicts the relationship between the energy, momentum and velocity of a high velocity charged particle, it is necessary to understand the differences between the laws of motion predicted by each model. Special relativity is based on two postulates - the first being that the laws of physics are true in all inertial reference frames, and the second being that the speed of light (c) is constant in all inertial reference frames. These two ideas have consequences on the behavior of massive particles moving close to the speed of light. They predict that a massive particle cannot exceed the speed of light, and that at speeds much lower than c relativistic effects yield the same predictions as Newtonian effects. The laws relating the three quantities of interest K, $\vec{v}$, and $\vec{p}$ are outlined below.

In Newtonian Mechanics, the momentum $\vec{p}$ and velocity $\vec{v}$ of a particle of mass m are related by the following equation:

$$\vec{p} = m\vec{v} \tag{1}$$
$$\tag{2}$$

The momentum $\vec{p}$ and kinetic energy K relationship for the same Newtonian particle is given by the following equation:

$$K = \frac{p^2}{2m} \tag{3}$$

In relativistic dynamics however, the momentum $\vec{p}$ of the same particle of mass m and its velocity $\vec{v}$ are related by the following modified equation:

$$\vec{p} = \gamma m\vec{v} \tag{4}$$
$$\tag{5}$$

where the Lorentz factor $\gamma = \sqrt{1-\beta^2}$ is given in terms of relativistic beta $\beta := \frac{v}{c} = \frac{E}{B}$. We will use this definition of β further in the description of our results. The kinetic energy K and momentum $\vec{p}$ of the same particle are related by the relativistic model in the following manner:

$$K = mc^2(\sqrt{1+(\frac{p}{mc})^2} - 1) \tag{6}$$

In order to determine which model correctly predicts the relationships between K, $\vec{p}$ and $\vec{v}$ for a charged particle moving at high velocity, it is necessary to measure these individual quantities and extract their relationship for just such an object.

II. EXPERIMENTAL SETUP

In order to extract the relationships between K, $\vec{p}$ and $\vec{v}$ and determine which of the two models predicts the high velocity dynamics of a charged particle best, we subject a high energy electron to a magnetic and electric field and measure its kinetic energy, momentum and velocity. The equipment used to do so in this experiment consists of a spherical magnet containing a vacuum chamber within. The spherical magnet generates an approximately uniform magnetic field downwards within its hollow interior and was constructed based on the schematics outlined in the following paper[2]. Fluctuation in magnetic field was accounted for by measuring field strength at individual points within the sphere, and the standard deviation of these measurements was taken as the uncertainty in the magnetic field $\sigma_B = \pm 0.57$G at any point. The vacuum chamber within makes up the brunt of our apparatus and is shown in Fig. 1.

* ericrc@mit.edu

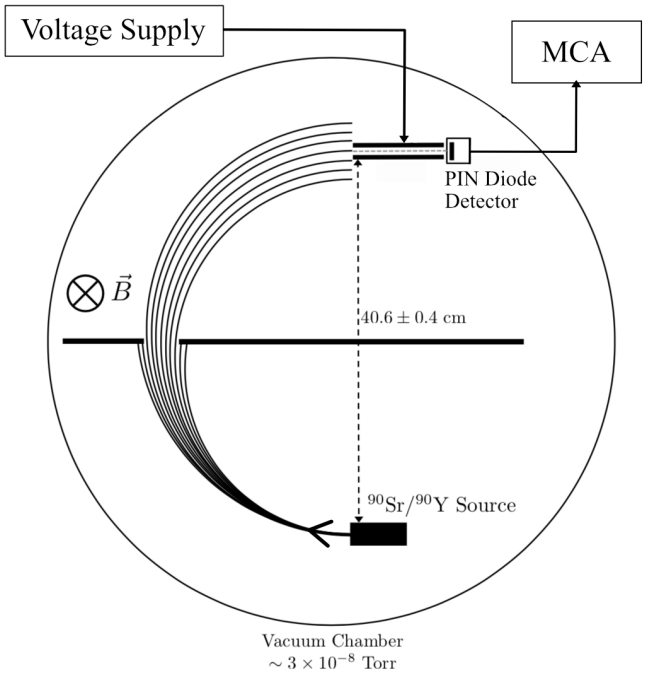

FIG. 1. A birds eye view of the vacuum chamber contained within the spherical magnet. The signal chain used to amplify and process the voltage output of our PIN Detector leading to our MCA is omitted for simplicity. Adapted from [3].

II.1. Radioactive Source and Baffling

High energy electrons are emitted from the decay of a ^{90}Sr source to ^{90}Y. Decay of ^{90}Sr emits an electron with a maximum energy of $0.546MeV$, and the ^{90}Y produced from this initial decay emits its own electron with a maximum energy of $2.27MeV$ [3]. Our source therefore produces electrons with a range of energies within 0 to $2.27MeV$. We position our source a radius $\rho = (20.3 \pm 0.4)\ cm$ away from our detector.

The magnetic field $\vec{B}$ produced by the spherical magnet encasing the vacuum chamber exerts a force on each electron that causes it to travel a circular path. Before proceeding further, it is relevant to mention that the total force on a particle due to a magnetic field $\vec{B}$ and an electric field $\vec{E}$ can be calculated using the Lorentz force law, which is derived from electromagnetic dynamics and holds in both relativistic and classical models.

$$\vec{F} = q(\vec{E} + (\frac{\vec{v}}{c}) \times \vec{B}) \tag{7}$$

Now, the momentum $\vec{p}$ of an electron travelling a circular path of radius ρ can be calculated by setting the centripetal force equal to the force exerted by the magnetic field to find:

$$p = mv = \frac{e\rho B}{c} \tag{8}$$

This equation demonstrates that fixing the magnetic field $\vec{B}$ and path radius ρ also fixes the momentum of a charged particle moving through our apparatus. In order to fix the path radius ρ, a metal baffle is placed at the center of the path with a small opening a radius $\rho = (20.3 \pm 0.4)\ cm$ from the center of the circle travelled by the electron. This small opening limits the radius of circular paths permitted through, thus isolating the momentum of a detected particle at a fixed magnetic field.

II.2. Velocity Selector and PIN Diode Detector

The velocity selector consists of two parallel metal plates separated by a distance $d = (0.180 \pm 0.003)\ cm$ positioned in front of the detector. In order to isolate the velocity of the electrons detected, we set a voltage difference between these two plates. In order for an electron to travel a straight path through the plates and reach the detector, the forces exerted on it by the electric field $\vec{E}$ across the plates and the magnetic field $\vec{B}$ exerted by the sphere must cancel. Using Faraday's Law to obtain $E = \frac{V}{d}$, we use the magnetic field force described in eq.8 and eq. 7 to derive the equation for a detected electron's velocity $v = \frac{Ec}{B}$.

Our detector is a PIN Diode detector covered by a thin film of aluminized mylar. It transmits voltage pulses which are then amplified by both a preamplifier and amplifier before being binned in a Multichannel Analyzer (MCA). The MCA displays a peak for each energy deposited from which the kinetic energy K of detected electrons can be extracted.

III. PROCEDURE

III.1. Barium Calibration

In order to extract kinetic energy from MCA data, a linear association between MCA channel number and energy must be found. In order to extract this relationship for this specific apparatus, a Barium 133 source with a well known energy emission spectrum was placed inside the vacuum chamber for 3 days. The log scaled MCA readout of this run is shown in Fig. 2. A Gaussian was fit to each peak of known energy, and the mean and uncertainty on the mean were taken as the channel number corresponding to the energy at that peak and the uncertainty on that channel number, respectively. By fitting a line to each extracted point and shifting both endpoints by their individual uncertainties to find an upper bound on the uncertainty of this fit, the following linear relationship between MCA channel number n and energy K was found: $K = (0.286 \pm 0.005)x + (0.558 \pm 0.28)$.

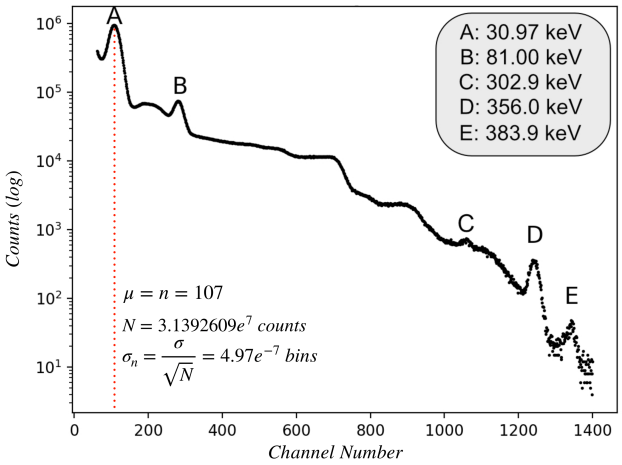

FIG. 2. A log scaled MCA plot of our Barium emission spectrum with the 5 most prominent peaks and their associated energies labelled.

III.2. Central Voltage Determination

In order to isolate detected particle velocity as discussed, it was necessary to find the optimal voltage to apply to the velocity selector at each individual magnetic field. For each magnetic field from 80G to 110G in increments of 5G, a range of voltages were applied across the velocity selector plates. For each voltage the total number of counts registered within a fixed channel window centered around the energy peak were recorded. In order to find the optimal voltage that let the highest number of electrons through, these counts were plotted as a function of voltage for each field, and a Gaussian fit was performed treating each count as a Poisson random variable. The mean of this Gaussian was determined to be the central voltage at a specific magnetic field, and the uncertainty on the mean was taken to be the uncertainty in this central voltage. These uncertainties ranged from $\pm 0.11\ keV$ to $\pm 0.15\ keV$.

IV. RESULTS AND ANALYSIS

After extracting a relationship between energy K and channel number n, and determining central voltages for each field, measurements were performed by gathering MCA spectra for 30 minutes for each magnetic field from 80G to 110G in increments of 5G. From this data we determine the fit to a specific model and extract the electron charge to mass ratio $\frac{e}{m_e}$.

IV.1. Plot of β vs. $\vec{B}$

In order to determine which theoretical model predicts the observed outcome, we plot $\beta = \frac{E}{B} = \frac{V_c}{dB}$ for velocity selector voltage V_c and distance d against magnetic field B in order to relate electron velocity $\vec{v}$ and momentum $\vec{p}$. Newtonian mechanics predicts that $\beta = \frac{e\rho B}{mc^2}$, while relativistic dynamics predicts that $\beta = \sqrt{\frac{a^2}{1+a^2}}$ where $a = \frac{e\rho B}{mc^2}$. This plot is shown in Fig. 3.

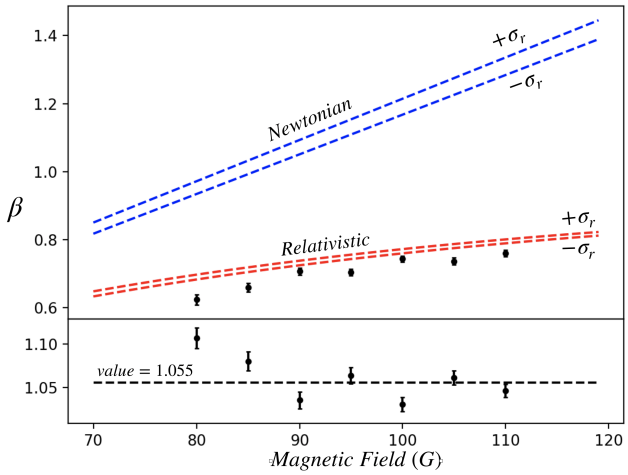

FIG. 3. $\beta = \frac{v}{c}$ vs. magnetic field $\vec{B}$ with error bands for each model prediction, and residuals plotted below for the values of $f = \frac{\beta_{relativistic}}{\beta_{data}}$ for each magnetic field. Note that the Newtonian curve predicts no upper bound on velocity v, and that the Relativistic curve diverges from the Newtonian curve as v approaches c.

The Relativistic model clearly provides the better fit to the observed data, while the Newtonian model lies multiple sigma away. In order to quantify correlated systematic uncertainty on each model prediction stemming from path radius ρ, $\sigma_{rho} = \pm 0.4\ cm$ is propagated individually to obtain an offset of $\pm 1.97\%$ for each curve. Uncertainty in the value of $d = (0.180 \pm 0.003)\ cm$ produces a $\pm 1.67\%$ correlated offset for each data point. Propagated uncertainties $\sigma_{voltage}$ due to uncertainty in velocity selector voltages are as follows for each magnetic field from 80G to 110G in increasing order: 1.49%, 1.28%, 1.05%, 0.97%, 0.89%, 1.03%, 1.01%. Normalization uncertainty on the relativistic fit and observed data due to magnetic field was quantified by extracting the ratio $f = \frac{\beta_{relativistic}}{\beta_{data}}$, and plotting the residuals with uncertainty $\sigma_{resid} = \frac{df}{dB}\sigma_B$. Fitting a constant to these residuals with $\chi^2_{pdf} = 1.22$ for 6 degrees of freedom yields a normalization error of 5.5% with uncertainty ranging from $\pm 0.8\%$ to 1.5% based on point.

IV.2. Extracting $\frac{e}{m_e}$

The electron charge to mass ratio was extracted from collected data. The Newtonian model predicts $(\frac{e}{m})_{Newtonian} = \frac{\beta c^2}{Br}$ for magnetic field B and velocity selector electric field E. Relativistic dynamics predicts

$(\frac{e}{m})_{Relativistic} = \frac{\beta c^2}{Br\sqrt{1-\beta^2}}$. For each value of $\beta = \frac{V_c}{l}dB$ observed in the experiment, a point was plotted for the relativistic prediction and Newtonian prediction. Each model was fit with a constant to determine the its prediction of the charge to mass ratio based on data collected, as shown in Fig. 4.

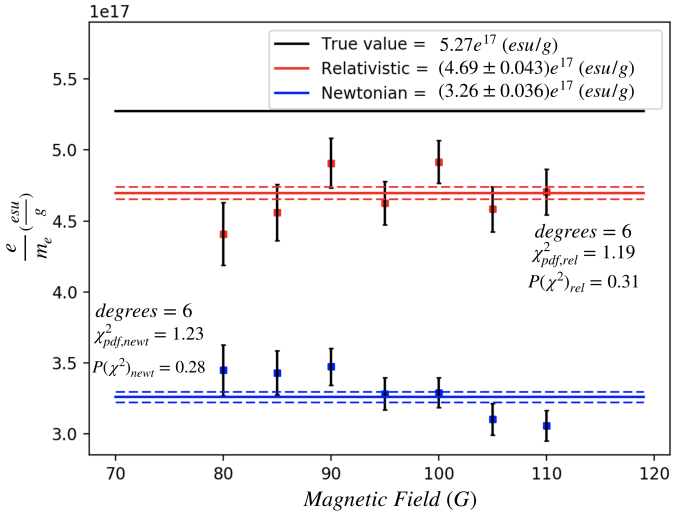

FIG. 4. A plot of relativistic and Newtonian predictions for $\frac{e}{m_e}$. Constant fits are drawn with dotted lines above and below to illustrate uncertainty.

For each model at each magnetic field, uncertainty in electric field $= \frac{V_c}{d}$ and magnetic field $\vec{B}$ are propagated in quadrature to obtain the following uncertainties on each predicted charge to mass ratio value: $\sigma_{\frac{e}{m_e},Newtonian} = (\sqrt{\sigma_E^2 + 4\sigma_B^2})(\frac{e}{m_e})$ and $\sigma_{\frac{e}{m_e},Relativistic} = (\sqrt{\sigma_E^2 + \sigma_B^2})(\frac{e}{m_e})$. Each constant fit carries an uncertainty determined by performing a Monte Carlo simulation. Each individual extracted $\frac{e}{m_e}$ data value is varied by an amount raffled at random from within its uncertainty. A fit is then performed on each set of randomly shifted points, and the standard deviation of the residuals between each random fit and the original extracted fit yields uncertainties for each models prediction. The final predicted values are $(\frac{e}{m})_{Relativistic} = (4.69 \pm 0.043)e^{17}$ (esu/g) and $(\frac{e}{m})_{Newtonian} = (3.26 \pm 0.036)e^{17}$ (esu/g), compared to the true charge to mass ratio of $5.27e^{17}$ (esu/g)[4].

IV.3. Plot of K vs. $\vec{p}$

Lastly, it is important to briefly mention the relationship between kinetic energy K and momentum $\vec{p}$ achieved by plotting the two as shown in Fig. 5. Relativistic and Newtonian predictions for K are given by $K_{Newtonian} = \frac{p^2}{2m}$ and $K_{Relativistic} = \sqrt{m^2c^4 + c^2p^2} - mc^2$. The kinetic energy is extracted for each field from collected MCA data by fitting a Gaussian to the energy peak, and passing each mean channel number into the linear relationship extracted from the Barium calibration described earlier yields the associated kinetic energy. This plot again shows the adherence of observed data to the relativistic prediction, and serves to reinforce the conclusion achieved by plotting β against $\vec{B}$. For a more in depth analysis of this plot, please refer to my lab partner Matthew Johnston's paper addressing the subject[5].

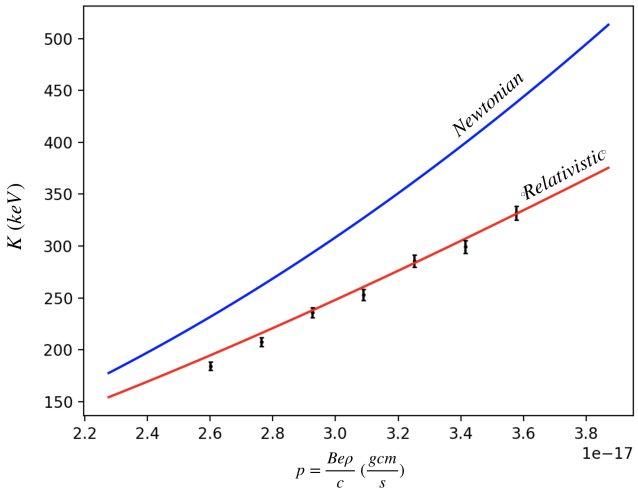

FIG. 5. A plot of kinetic energy against momentum, demonstrating again the adherence of observed data to the relativistic model prediction.

V. CONCLUSIONS

We now see an significant consequence of Einstein's theoretical predictions. The dynamics of bodies moving at high speeds close to c evade accurate prediction through classical means, and relating the energy, momentum and velocity of such a body requires the relativistic model. From this model's predictions we can extract the charge to mass ratio $(\frac{e}{m})_{relativistic} = (4.69 \pm 0.043)e^{17}$ (esu/g), against a true value of $5.27e^{17}$ (esu/g)[4].

ACKNOWLEDGMENTS

We gracefully thank Prof. Hen and the entire 8.13 staff for their continued support and guidance throughout the course of this experiment.

[1] A. Einstein *et al.*, Annalen der Physik **17**, 50 (1905).
[2] J. W. Clark, Review of Scientific Instruments **9**, 320322 (1938).
[3] . Staff, "Relativistic dynamics lab guide,".
[4] "Codata electron charge to mass ratio," .
[5] M. Johnston, "Relativistic dynamics,".